Journal of Biomolecular Structure and Dynamics

ISSN: 0739-1102 (Print) 1538-0254 (Online) Journal homepage: http://www.tandfonline.com/loi/tbsd20

Multi-drug resistance profile of PR20 HIV-1 protease is attributed to distorted conformational and drug binding landscape: molecular dynamics insights

Sarentha Chetty, Soumendranath Bhakat, Alberto J.M. Martin & Mahmoud E.S. Soliman

To cite this article: Sarentha Chetty, Soumendranath Bhakat, Alberto J.M. Martin & Mahmoud E.S. Soliman (2016) Multi-drug resistance profile of PR20 HIV-1 protease is attributed to distorted conformational and drug binding landscape: molecular dynamics insights, Journal of Biomolecular Structure and Dynamics, 34:1, 135-151, DOI: 10.1080/07391102.2015.1018326

To link to this article: http://dx.doi.org/10.1080/07391102.2015.1018326

Journal of Biomolecular Structure and Dynamics, 2016
Vol. 34, No. 1, 135–151, http://dx.doi.org/10.1080/07391102.2015.1018326

Taylor & Francis
Taylor & Francis Group

Multi-drug resistance profile of PR20 HIV-1 protease is attributed to distorted conformational and drug binding landscape: molecular dynamics insights

Sarentha Chetty[a,1], Soumendranath Bhakat[a,1], Alberto J.M. Martin[b,c] and Mahmoud E.S. Soliman[a]*

[a]*Molecular Modelling and Drug Design Research Group, School of Health Sciences, University of Kwazulu-Natal, Westville, Durban 4000, South Africa;* [b]*Computational Biology Lab, Fundación Ciencia & Vida, Santiago, Chile;* [c]*Facultad de Ciencias, Centro Interdisciplinario de Neurociencia de Valparaíso, Universidad de Valparaíso, Valparaíso, Chile*

Communicated by Ramaswamy H. Sarma

(*Received 28 October 2014; accepted 8 February 2015*)

The PR20 HIV-1 protease, a variant with 20 mutations, exhibits high levels of multi-drug resistance; however, to date, there has been no report detailing the impact of these 20 mutations on the conformational and drug binding landscape at a molecular level. In this report, we demonstrate the first account of a comprehensive study designed to elaborate on the impact of these mutations on the dynamic features as well as drug binding and resistance profile, using extensive molecular dynamics analyses. Comparative MD simulations for the wild-type and PR20 HIV proteases, starting from bound and unbound conformations in each case, were performed. Results showed that the apo conformation of the PR20 variant of the HIV protease displayed a tendency to remain in the open conformation for a longer period of time when compared to the wild type. This led to a phenomena in which the inhibitor seated at the active site of PR20 tends to diffuse away from the binding site leading to a significant change in inhibitor–protein association. Calculating the per-residue fluctuation (RMSF) and radius of gyration, further validated these findings. MM/GBSA showed that the occurrence of 20 mutations led to a drop in the calculated binding free energies (ΔG_{bind}) by ~25.17 kcal/mol and ~5 kcal/mol for p2-NC, a natural peptide substrate, and darunavir, respectively, when compared to wild type. Furthermore, the residue interaction network showed a diminished inter-residue hydrogen bond network and changes in inter-residue connections as a result of these mutations. The increased conformational flexibility in PR20 as a result of loss of intra- and inter-molecular hydrogen bond interactions and other prominent binding forces led to a loss of protease grip on ligand. It is interesting to note that the difference in conformational flexibility between PR20 and WT conformations was much higher in the case of substrate-bound conformation as compared to DRV. Thus, developing analogues of DRV by retaining its key pharmacophore features will be the way forward in the search for novel protease inhibitors against multi-drug resistant strains.

Keywords: HIV protease; PR20; flap dynamics; conformational flexibility; binding free energy; residue interaction network

1. Introduction

The use of highly active anti-retroviral treatments has had a major influence on improving prognosis outcomes for HIV-infected patients. The rapid development of drug resistance, however, firmly retains HIV/AIDS in the public health spotlight (http://www.who.int/topics/hiv_aids/en/). The emergence of multi-drug resistance threatens to reduce the effectiveness of currently available drug regimens, posing a serious challenge to treatment decisions and options. Resistance as a result of mutations is largely attributed to the transcriptional errors of the HIV reverse transcriptase, as well as selective drug pressure, altering the catalytic activity of HIV protease (PR) (Agniswamy et al., 2012, 2013; Bennett et al., 2009; Flexner, 2007).

HIV protease is one of the main targets for anti-retroviral drugs. Structurally, HIV PR is a homo-dimer, and the active site containing a conserved triad (Asp25-Thr26-Gly27) is located at the dimer interface of two proteases (Figure 1(A)). The Asp (Asp25 and Asp25′) residue from each monomer (Brik & Wong, 2003; Mehellou & De Clercq, 2010; Wlodawer & Vondrasek, 1998) plays a crucial role in holding the substrate in place. An open conformation of the dimer is required to accommodate an incoming substrate, with subsequent binding leading to a closed conformation. Two flexible flaps comprising residues 44–57 control the entrance to this active site.

Major mutations in the HIV-PR can lead to a serious decrease in binding affinity of protease inhibitors (PIs) or natural substrates, as well as impair viral replication (Molla et al., 1996; Muzammil, Ross, & Freire, 2003; von der Helm, 1996; Zhang et al., 1997). Drug resistance

*Corresponding author. Email: soliman@ukzn.ac.za
[1]Authors contributed equally.

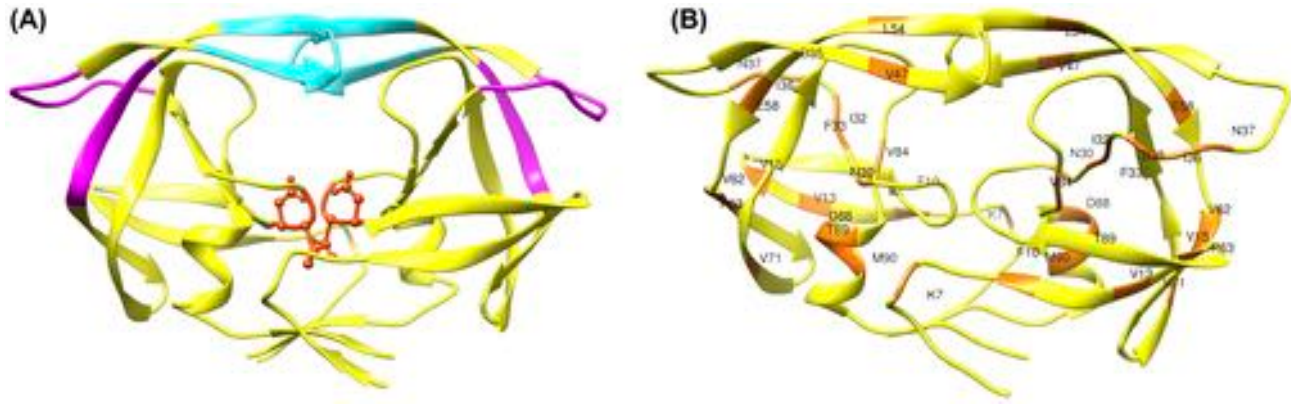

Figure 1. (A) The structure of HIV protease. The flaps (residues 46–54) and hinge regions (residues 35–42 and 57–61) are shown in cyan and magenta, respectively. The catalytic triad residues (25, 26 and 27) are presented in an orange ball and stick representation. (B) The structure of the PR20 variant of the HIV protease. The location of PR20 mutations are highlighted in "orange" and labelled with residue identifiers.

can also occur through the addition of up to six amino acids at different sites or via mutations that can occur in the PR cleavage sites of the Gag precursor. To date, 15 major and 19 minor mutation sites have been determined (Agniswamy et al., 2012). Furthermore, the protease inhibitors that are currently available share structural similarity, which substantially increases the likelihood for cross-resistance (Rhee et al., 2010).

Recently, Agniswamy et al. (2012, 2013) identified a multi-drug resistant (MDR) mutant (PR20) variant of HIV-PR, which has 20 mutations. These mutations, Q7K, L10F, I13V, I15V, D30N, V32I, L33F, E35D, M36I, S37N, I47V, I54L, Q58E, I62V, L63P, A71V, I84V, N88D, L89T and L90M (Figure 1(B)), have made the enzyme extremely resistant to all clinical available protease inhibitors (PIs). The autocatalytic activity of this mutated enzyme, even in the presence of protease inhibitors, however, interestingly, remains unaltered. Fifteen of these mutations could be classed as either major or minor site mutations (Agniswamy et al., 2012, 2013). The D30N, V32I, I47V and I84V mutations alter direct interactions with darunavir (DRV) and saquinavir (SQV), whereas the Q7K, L10F, L33F, I54L, N88D and L90M mutations influence the residues that interact with the inhibitor within the active site (Agniswamy et al., 2012). Regions on the PR20 mutant that contain major drug resistant mutations as defined by the Stanford database (http://hivdb.stanford.edu/) are residues: D30N, V32I, L33F, I54L, I84V, N88D and L90M.

It has been reported that mutations affecting the dynamics and flexibility of the flaps would have an influence on inhibitor binding as well as the catalytic activity of the enzyme (Agniswamy et al., 2012; Foulkes-Murzycki, Rosi, Yilmaz, Shafer, & Schiffer, 2013; Heal, Jimenez-Roldan, Wells, Freedman, & Romer, 2012; Leonis, Steinbrecher, & Papadopoulos, 2013; Liu et al., 2008; Naicker et al., 2013; Scott & Schiffer, 2000).

Investigation into the conformational flexibility of the HIV-PR using computational tools has been well described in the literature (Hornak, Okur, Rizzo, & Simmerling, 2006a, 2006b; Perryman, Lin, & McCammon, 2004). An understanding of flap dynamics is a crucial aspect in order to interpret the overall conformational flexibility and ligand binding landscape. Various computational and experimental studies, e.g. MD simulation (Hornak et al., 2006a; Hornak, Okur, Rizzo, & Simmerling, 2006c; Karthik & Senapati, 2011), NMR (Freedberg et al., 2002) and X-ray crystallography (Hornak & Simmerling, 2007), have been applied to investigate the flap opening and closing mechanism of HIV protease. The flaps play a major role in ligand binding by drawing the incoming ligand inwards followed by subsequent closure, retaining the ligand within the active site (Hornak et al., 2006a). Experimentally, two main flap conformations were observed; one is of the ligand bound in a closed conformation and another is of a semi-open apo conformation (Hornak et al., 2006a). Several computational studies using different force fields and solvation models were also used to provide insight into HIV protease flap dynamics (Hornak et al., 2006a, 2006b; Karthik & Senapati, 2011).

Several metrics have been proposed to describe transition in various flap conformations of HIV protease. The most commonly used metric is based on calculating the distance between C-alpha carbons of Ile50 and Ile149 (Heaslet et al., 2007; Hornak et al., 2006a; Zhu, Schuster, & Tuckerman, 2003). This distance was observed to fluctuate between 5 and 30 Å depending on the closed, semi-open and fully opened conformations of HIV protease (Hornak et al., 2006a).

We previously reported the first account of flap flexibility of the unbound C-SA HIV protease using

X-ray crystallography and explicit solvation molecular dynamics simulations (Naicker et al., 2013). The flap flexibility was measured by calculating the distance between C-alpha carbons of residues Ile50 and Ile149 (Naicker et al., 2013). The effects of mutation(s) on flap dynamics as well as inhibitor binding have been reported in several publications (Ahmed, Maguire, Kruger, & Govender, 2014; Foulkes-Murzycki et al., 2013; Leonis et al., 2013; Liu et al., 2008; Scott & Schiffer, 2000; Zhang et al., 2014).

The impact of the 20 mutations in the MDR PR20 HIV PR on the flap flexibility, overall enzyme dynamics and inhibitor binding and resistance at an atomistic level is lacking in the literature; therefore, we embarked on this study. The current report aims to provide a comparative and comprehensive multi-dimensional picture of the impact of the PR20 mutations on the conformational, drug binding and resistance landscape. To accomplish this, a comparative molecular dynamics study for the wild-type HIV-PR and PR20 variant, in their unbound and bound conformations, was carried out. To ensure the structural diversity of the inhibitors, we used two different ligands: natural peptidomimetic substrate, p2-NC (Tie et al., 2005) and a second-generation HIV protease inhibitor, darunavir (DRV) (Figure 2). Unliganded (created by manual deletion of inhibitor) structures of both wild and PR20 variant of HIV proteases were also simulated as a direct control to validate the dynamic changes that occurred in the case of the apo conformations (Hornak et al., 2006a). For each system, a 50 ns all-atom molecular dynamics simulation was performed, followed by a wide range of post-dynamics analyses (Section 2.2).

The findings reported in this study will be important to understand the specific changes that occur due to the PR20 mutations as well as to gain insight into the mechanism of drug resistance, knowledge of which would be valuable in the design of new HIV drugs.

2. Computational methodology

2.1. System preparations

The simulated systems, crystal structures (protein data bank (PDB) codes) and corresponding abbreviations are listed in Table 1.

All systems were retrieved from the PDB and prepared as detailed in our previous reports (Bhakat, Martin, & Soliman, 2014; Karubiu, Bhakat, & Soliman, 2014). To generate the unliganded structures, inhibitors were manually deleted from the crystal structures of complexes. A total of eight systems (Table 1) were subjected to a 50 ns molecular dynamics simulation as described in Section 2.2.

2.2. Molecular dynamics and post-dynamics analyses

All-atom 50 ns molecular dynamics simulations and post-dynamics analyses including RMSF, RMSD, inter-residue distance, potential energy, radius of gyration, solvent-assessable surface area (SASA) and principal component analysis (PCA) were performed using the standard parameters and methods described in our previous reports (Ahmed et al., 2013; Bhakat et al., 2014; Karubiu et al., 2014; Naicker et al., 2013). The H^{++} server (http://biophysics.cs.vt.edu/H++) was used to assign correct protonation states in the case of all the receptors prior to system preparation. In brief, the geometry of the ligands was optimized at HF/6-31G* level using Gaussian 09. Finally, the antechamber module was used in order to generate atomic partial charges for all the ligands using RESP and force field parameters of GAFF. The FF99SB force field integrated with Amber 12 was used to describe the protein systems. The systems were then processed using typical parameters described by Bhakat et al. (2014) and Karubiu et al. (2014). The minimization steps were performed using the CPU version of the PMEMD engine provided with Amber 12 whereas the heating and equilibration steps were carried out using the GPU version of PMEMD engine integrated with Amber 12. Finally, MD production runs were performed using the GPU version of PMEMD engine provided with Amber 12 (Case et al., 2005). The trajectories were saved every 1 ps and analysed using the PTRAJ and CPPTRAJ modules (Roe & Cheatham III, 2013) integrated within Amber 12. MM/GBSA-based binding free energy calculations were performed using a singular trajectory approach on 1000 snapshots at equal intervals of 50 ps. Residue interaction network (RIN) was performed using RIN Analyzer (Doncheva, Klein, Domingues, & Albrecht, 2011) plug-in integrated with Cytoscape (Bauer-Mehren, 2013) as described in our previous reports. The probability of NMR mobility was performed using the ESpritz server (Walsh, Martin, Di Domenico, & Tosatto, 2012).

Visualizations were carried out using the graphical user interface of UCSF Chimera (Pettersen et al., 2004). The plots were generated using Origin data analysis software and Xmgrace (Makatini et al., 2013).

3. Results and discussion

3.1. Molecular dynamics and systems stability

The C-α backbone (RMSD) and potential energy fluctuations were monitored throughout the simulation period in order to ensure the stability of the simulated systems, and hence the accuracy of subsequent post-dynamic analyses. The RMSD and potential energy terms were found to be stable for all systems, thus ensuring system

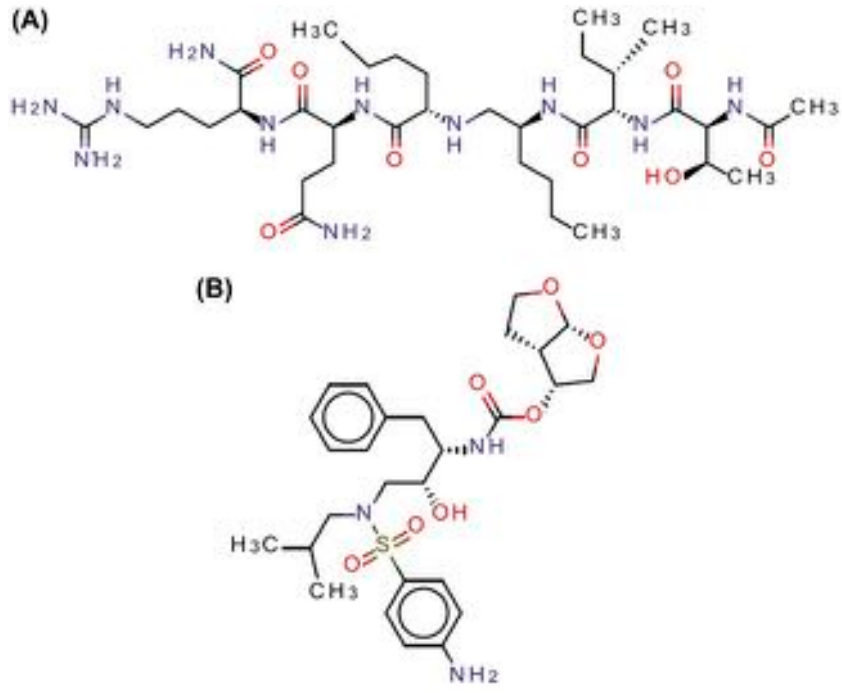

Figure 2. 2D structural representation of natural peptidomimetic substrate, p2-NC (A) and darunavir (B).

Table 1. The crystal structures of the simulated systems, PDB codes and abbreviations.

Simulated system	PDB code	Abbreviation[a]
Apo wild type	1HHP (Spinelli, Liu, Alzari, Hirel, & Poljak, 1991)	WT_{apo}
Substrate-bound wild type	2AOD (Tie et al., 2005)	WT_{Sub}
Darunavir-bound wild type	4DQB (Mittal, Cai, Nalam, Bolon, & Schiffer, 2012)	WT_{DRV}
Unliganded darunavir-bound wild type	4DQB[b]	WT_{unlig}
Apo PR20	3UF3 (Agniswamy et al., 2012)	$PR20_{apo}$
Substrate-bound PR20	3UHL (Agniswamy et al., 2012)	$PR20_{Sub}$
Darunavir-bound PR20	3UCB (Agniswamy et al., 2012)	$PR20_{DRV}$
Unliganded PR20	3UCB[b]	$PR20_{unlig}$

[a]These abbreviations are used throughout the manuscript.
[b]Unliganded conformation was generated by removing the inhibitor from active site.

equilibration for all systems during the simulation period (Supplementary Materials, Figures S1–S2).

3.2. *Investigation of the dynamic features of simulated PRs*

3.2.1. *Flap flexibility*

3.2.1.1. Apo conformations (WT_{apo} vs. $PR20_{apo}$). Flap dynamics play an integral role in the mechanism of the HIV protease. The design of new inhibitors, which are able to interfere with flap opening and closing, would therefore influence enzyme function. Understanding the mechanism of flap dynamics is, therefore, essential to the design of novel drug inhibitors that could affect this process (Piana, Carloni, & Rothlisberger, 2002). Hornak et al. (2006a) studied the flap dynamics of the apo and unliganded conformations of the HIV wild-type protease and observed a spontaneous opening and closing phenomena in the apo conformation of the HIV protease. Perryman et al. (2004) also demonstrated that an alteration in flap dynamics occurred, in the presence of mutation, in a ligand-bound conformation of the HIV-PR. The flap behaviour in the PR20 variant of the HIV-PR, to our knowledge, has not been previously reported. The starting structures of WT_{apo} (PDB: 1HHP) and $PR20_{apo}$ (PDB: 3UF3) conformations were crystallized in a semi-open conformation (Agniswamy et al., 2012) (Figure 3).

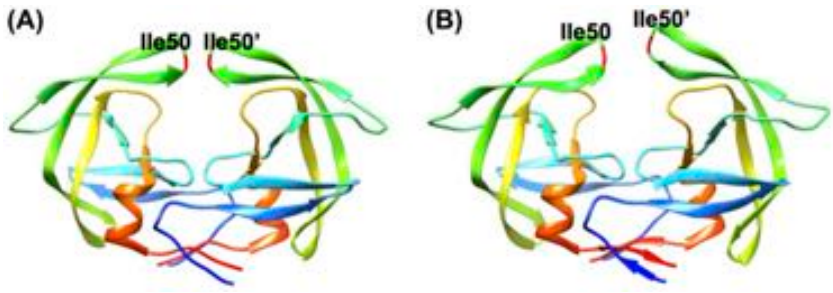

Figure 3. Starting conformations of the WT_{apo} (A) and the $PR20_{apo}$ (B) of HIV-1 protease. Flap tip residues Ile50 and Ile50′ are highlighted in red.

MD simulations showed that the average distance between flap tip residues was significantly greater in the case of the $PR20_{apo}$ variant when compared to WT_{apo} (Figure 4). Interestingly, the flap tips exhibited an open conformation for $PR20_{apo}$, occurring shortly within 5 ns of the total simulation time (vs. 20 ns in the case of WT_{apo}). Another interesting observation is that, while the flaps showed a two-cycle open-closure itinerary in the case of the WT_{apo} (Figure 5(A)), $PR20_{apo}$ remained in an asymmetrical open conformation for the entire duration of the 50 ns simulation (Figure 5(B)). Interestingly, one monomer (residues 100–198) showed a greater displacement from the initial starting conformation to the other (residues 1–99) (Figure 5(B)). The nature of flap dynamics of the WT_{apo} and $PR20_{apo}$ is in good accordance with the experimentally determined dimer dissociation constant (K_d), where $PR20_{apo}$ exhibited a 30-fold decrease in K_d when compared to WT_{apo} (Agniswamy et al., 2012, 2013). The asymmetrical nature of flap opening in the case of $PR20_{Apo}$ was further confirmed by the experimental evidence reported by Agniswamy et al. (2012). Such a noticeable difference in flap "tightness" causes enlargement of the binding site cavity and might significantly impact drug binding. It can be further postulated that as a result of a wide-open flap conformation, the inhibitor seated at the active site of PR20 tends to diffuse away from the binding site, leading to a significant change in inhibitor–protein association. This seems to complement the results obtained from MM/GBSA binding free energy calculations (Section 3.3).

3.2.1.2. Unliganded conformations (WT_{unlig} vs. $PR20_{unlig}$). In order to gain insight into the rigidity of the flaps, an approach similar to that of Hornak et al. (2006a) was adopted, in which manual removal of the ligand from the active sites of the PR complexes was performed to create systems for use as positive controls. As was the case with Hornak et al. (2006a), a similar observation occurred with our systems with that the starting conformation of the WT_{unlig} and $PR20_{unlig}$ remained in a closed conformation for the entire duration of the MD simulation (Figure 6).

3.2.2. Overall dynamics of HIV protease

3.2.2.1. Apo conformations (WT_{apo} vs. $PR20_{apo}$). The per-residue based fluctuation, also denoted as root mean square fluctuation (RMSF), of the WT_{apo} vs. $PR20_{apo}$ highlight the impact of the 20 mutations on the overall conformational flexibility and dynamics of the protein (Figure 7(A)). Figure 7(A) shows greater per-residue Cα fluctuations in the case of WT_{apo} as compared $PR20_{apo}$ (average magnitude of 1.21 and 1.52 Å for WT_{apo} and $PR20_{apo}$, respectively).

It is worth mentioning that upon visual inspection of the protein conformations ("snapshots") along the MD trajectory, we found that $PR20_{apo}$ exhibits an "asymmetrical" open conformation (Figure 5(B)) – as was observed by the larger per-residue fluctuation of one monomer (residues 100–198) over the other (residues 1–99) (Figure 7(A)). This phenomenon of "asymmetric" flap opening of PR20 variant could lead to significant changes in dimer association (validated by the fact that

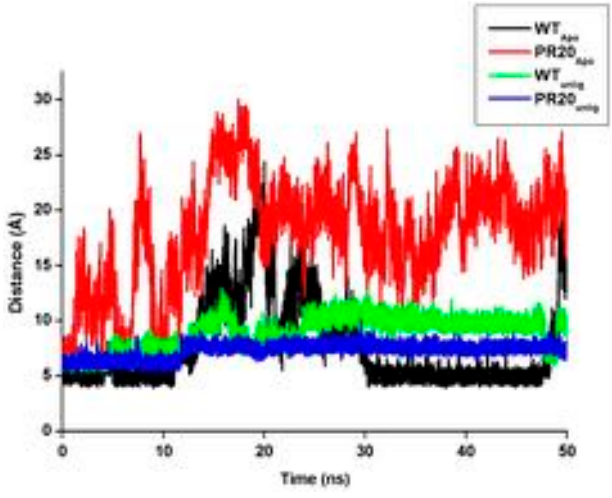

Figure 4. The distance between the C-alpha atoms of flap tip residues, Ile50–Ile149 during molecular dynamics simulation. Red, black, green and blue highlight fluctuation in distance for $PR20_{apo}$, WT_{apo}, WT_{unlig} and $PR20_{unlig}$, respectively.

the dimer dissociation constant (K_d) for $PR20_{apo}$ exhibited a 30-fold decrease when compared to WT_{apo} (Agniswamy et al., 2012)) and consequently on drug binding, hence the emergence of resistance.

The calculations of radius of gyrations were carried out at 300 K as described in our previous reports (Bhakat et al., 2014; Karubiu et al., 2014). Radius of gyration (R_g) is defined as the moment of inertia of the C-alpha atoms from its centre of mass. Figure 8(A) highlights the radius of gyration (R_g) for WT_{apo} and $PR20_{apo}$ conformations, respectively. The asymmetric flap opening of $PR20_{apo}$ conformation and the tendency of $PR20_{apo}$ to remain in an open conformation for a longer period of simulation time destabilizes the mass centre of $PR20_{apo}$ which increases the average R_g fluctuation (average R_g 19.48 Å) in comparison to WT_{apo} (average R_g 18.31 Å).

3.2.2.2. Substrate-bound conformations (WT_{Sub} vs. $PR20_{Sub}$). The effect of 20 mutations on the p2-NC (substrate) bound conformation of HIV-PR is an interesting aspect as it brings diversity of ligand selection into this study. In order to gain an understanding into the difference in hydrophobic compactness between WT_{Sub} and $PR20_{Sub}$, SASA were determined for both systems. The expanded conformation of $PR20_{Sub}$ was further confirmed by a larger breathing in the SASA (Figure 9(A)), signifying a loss in the hydrophobic compactness as a result of the 20 mutations.

The effect of 20 mutations on residue fluctuations can clearly be deduced from the RMSF plot. Figure 7(B) highlights the residue-based Cα fluctuation of the WT_{Sub} and $PR20_{Sub}$. Overall, the per-residue fluctuation (RMSF) of $PR20_{Sub}$ (average RMSF .94 Å) was much greater than that of WT_{Sub} (average RMSF .70 Å). A higher degree of fluctuation occurs in the case of $PR20_{Sub}$ within the residues ranging from 1 to 136, whereas a higher degree of fluctuation was also observed in the case of residues ranging from 136 to 145 and from 155 till residue 162. Residues 30–45 and 130–145 correspond to regions where mutations, Asp30Asn, Val32Ile, Leu33Phe, Glu35Asp, Met36Ile and Ser37Asn, occur – we presume occurrence of these major mutations in PR20 led to an overall increase in RMSF which led to significant decrease in binding free energy (Table 2) in the case of $PR20_{Sub}$, as a result of increasing flexibility which ultimately leads to an decreased grip of enzyme on substrate.

This trend in the per-residue fluctuation further remained somehow consistent with the RMSF outcome of the DRV-bound conformation of wild and PR20 variant HIV-PR (Section 3.2.2.3). But a major difference between DRV- and substrate-bound conformations is that in the case of WT_{DRV} and $PR20_{DRV}$, the average RMSF (Figure 7(C)) of WT_{DRV} is slightly higher than $PR20_{DRV}$ which is consistent with the fact that DRV is one of the drugs of choice targeting HIV-1 protease till date. It has a better binding free energy profile (Table 2) targeting PR20 as compared to substrate. The radius of gyration (R_g), presented in Figure 8(B), highlights the highly unstable nature of $PR20_{Sub}$. Often a larger deviation in R_g signifies the unstable moment of inertia of the bimolecular system. The $PR20_{Sub}$ exhibited a larger breathing in R_g with an average value of 17.98 Å as compared to WT_{Sub} (17.46 Å).

Eigenvalues extracted from principal component analysis (PCA) give an indication of the degree of fluctuation and mobility of the protein in a system (Kamaraj

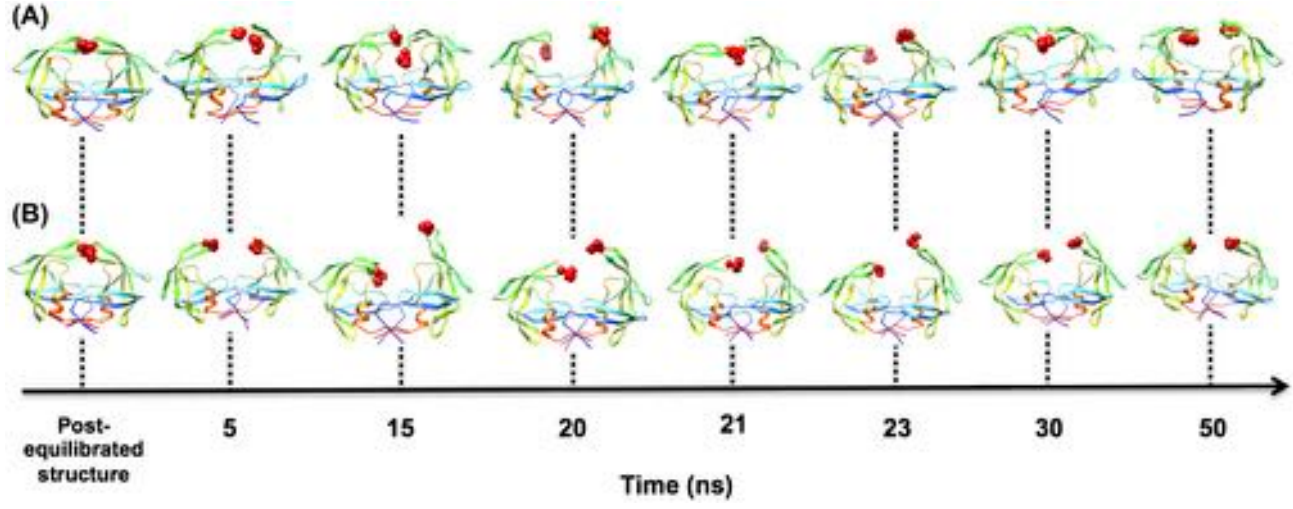

Figure 5. Snapshots along the simulation trajectory highlighting the opening and closing of HIV protease flaps. The red balls highlight the position of flap tip residues Ile50 and Ile149. A and B correspond to WT_{apo} and $PR20_{apo}$ conformations of HIV-PR.

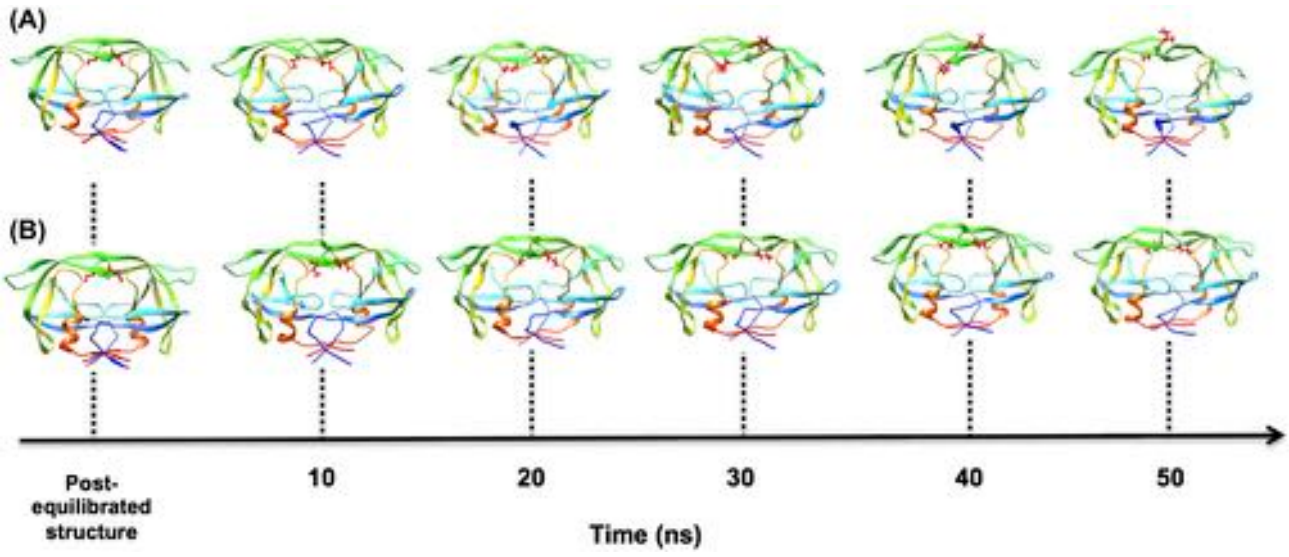

Figure 6. Snapshots taken along the simulation trajectory highlighting the position of the HIV protease flaps. The red sticks highlight the position of flap tip residues Ile50 and Ile149. A and B correspond to WT_{unlig} and $PR20_{unlig}$ conformations of HIV-PR, respectively.

& Purohit, 2013). The highest eigenvalues are normally found in the first few eigenvectors (Kamaraj & Purohit, 2013; Shenai & Zhao, 2012). PCA plots provide insight into the regions of the subspace that these eigenvectors occupy (Doss et al., 2014). Here, the principal component analysis highlighted a difference in motion between the native wild-type and the PR20 variant complexes across the first two principal components (Figure 10(A)). A residue-based mobility plot (Figure 11(A) and (B)) across the first two normal modes showed a slightly greater average fluctuation in the case of the $PR20_{Sub}$ (average mobility, NM1 4.21 Å and NM2 4.05 Å) with regard to both mode 1 (NM1) and mode 2 (NM2), as compared to WT_{Sub} (average mobility, NM1 3.92 Å and NM2 3.73 Å). The mobility plot highly corresponds with the RMSF outcome and provides solid reasoning for a decreased binding free energy in the case of $PR20_{Sub}$, as a result of a decreased grip of protein due to an increased flexibility.

3.2.2.3. Darunavir-bound conformations (WT_{DRV} vs. $PR20_{DRV}$). A study of the DRV-bound conformation of the wild and PR20 variant of the HIV-PR highlights the effect of the PR20 mutations on the inhibitor-bound landscape as well as the overall conformation of HIV-PR. Darunavir is the one of the most potent FDA approved HIV protease inhibitors to date; hence, an understanding into the mutational effect on darunavir binding, will help in developing more potent inhibitors to combat HIV. The fluctuation of RMSDs with minute differences in each case validated the stability of the wild and PR20 complexes during the process of simulation (Figure S1 in Supplementary Materials). It was observed that the deviations of the backbone Cα atoms were slightly higher in the case of the $PR20_{DRV}$ as compared to WT_{DRV}. This trend in RMSD fluctuation highly correlates with the RMSF fluctuation observed in the case of WT_{Sub} and $PR20_{Sub}$. The deviation in RMSD fluctuation further confirms destabilization of structural compactness as well as an expanded conformation as a result of the 20 mutations.

To gain an understanding into the influence of the PR20 mutations on conformational flexibility of the biomolecule, per-residue fluctuations (RMSF) during the simulation time were computed. Figure 7(C) shows the per-residue fluctuations of the Cα atoms during the simulation period. The average RMSF of WT_{DRV} (average RMSF .91 Å) was found to be slightly greater than $PR20_{DRV}$ (average RMSF .90 Å). This was contrary to the larger deviation observed in the case of substrate-bound conformation. This further substantiates the fact that the occurrence of 20 mutations leads to an increase in conformation flexibility, which leads to a decreased binding of ligand within the active site. Very slight differences in RMSF between WT_{DRV} and $PR20_{DRV}$ highly correlates with the predicted and experimental binding free energy which confirms DRV as the most potent drug against the PR20 variant.

The NMR flexibility of WT_{DRV} and $PR20_{DRV}$ conformations of HIV-PR using the ESpritz server (Walsh et al., 2012) confirmed a similar trend in percentage probability of mobility in the case of PR20DRV and WTDRV, though this calculation using static crystallographic snapshots carries little value in understanding

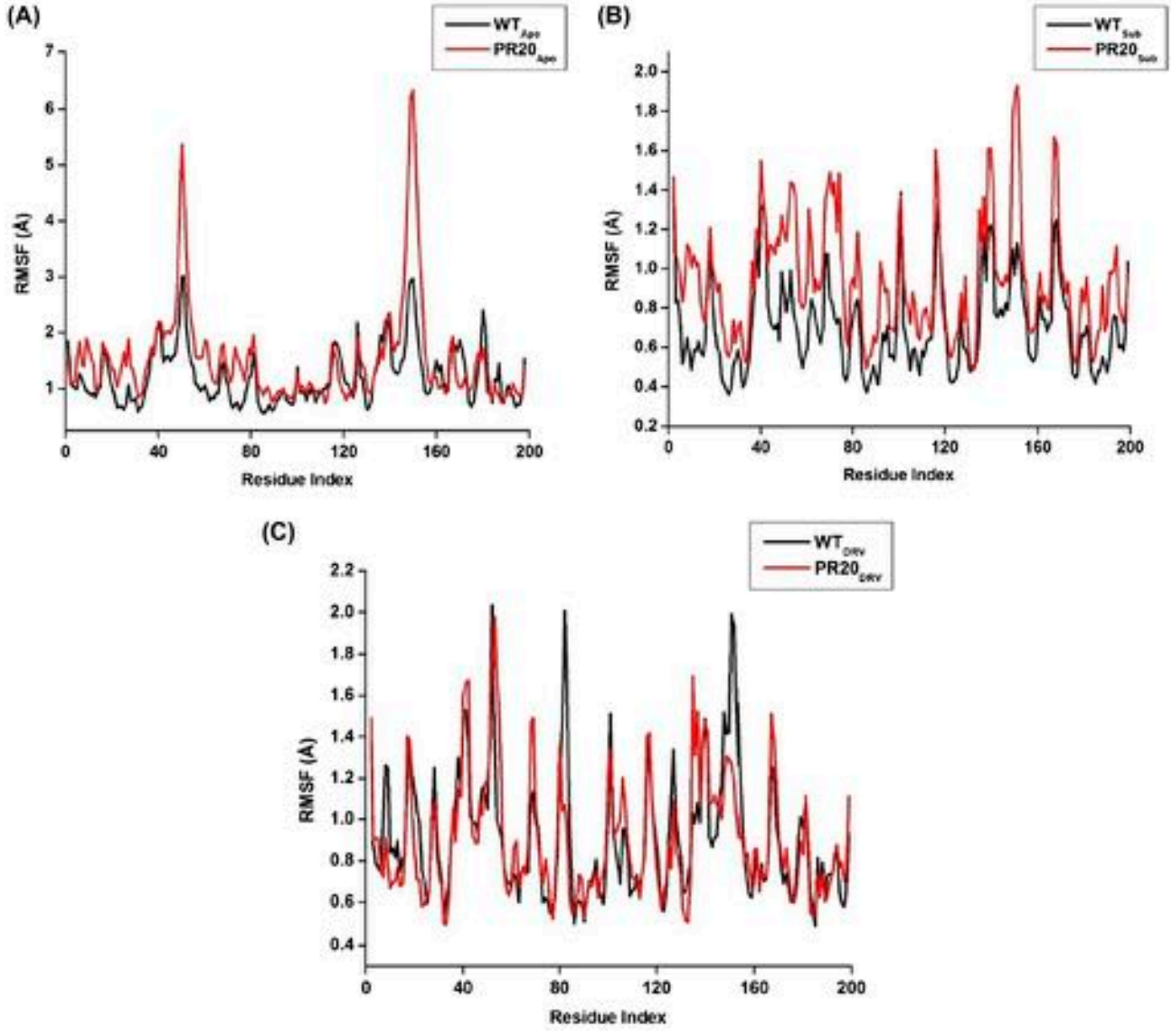

Figure 7. Per-residue C-α fluctuations of amino acid residues during the MD simulation. A, B and C highlight RMSF fluctuations in the case of the WT_{apo}/$Pr20_{apo}$, WT_{Subs}/$PR20_{Subs}$ and WT_{DRV}/$PR20_{DRV}$, respectively. The RMSF fluctuation is highly consistent with the trend of b-factor fluctuation (Figure S3, Supplementary Materials) during simulation time.

dynamical data motion (Figure S5 in Supplementary Materials).

The findings obtained from RMSF and NMR-based mobility studies were further justified by a larger average value of the radius of gyration (Figure 8(C)) in the case of the wild type (average $R_g = 17.73$ Å) as compared to the PR20 variant (average $R_g = 17.85$ Å). This data further suggest a more flexible conformational nature of the PR20 variant as compared to wild type.

The SASA gave an understanding into the compactness of the hydrophobic core of protein–ligand systems. It was observed that the average SASA was slightly higher in the case of $PR20_{DRV}$ as compared to its wild-type counterpart (Figure 9(B)). This larger breathing in SASA suggests destabilization of the hydrophobic core area of HIV-PR as a result of 20 mutations. Destabilization of hydrophobic core directly affects evolution of inhibitor in its active site and ultimately contributes towards resistance.

PCA was carried out for both WT_{DRV} and $PR20_{DRV}$ complexes in order to gain an understanding into the effect of mutation on the overall motion of both systems. Figure 10(B) highlights the projection of the overall motion along the first two principal components. The PCA plot highlights a significant difference in eigenvalues for the WT_{DRV} and $PR20_{DRV}$ complexes. The

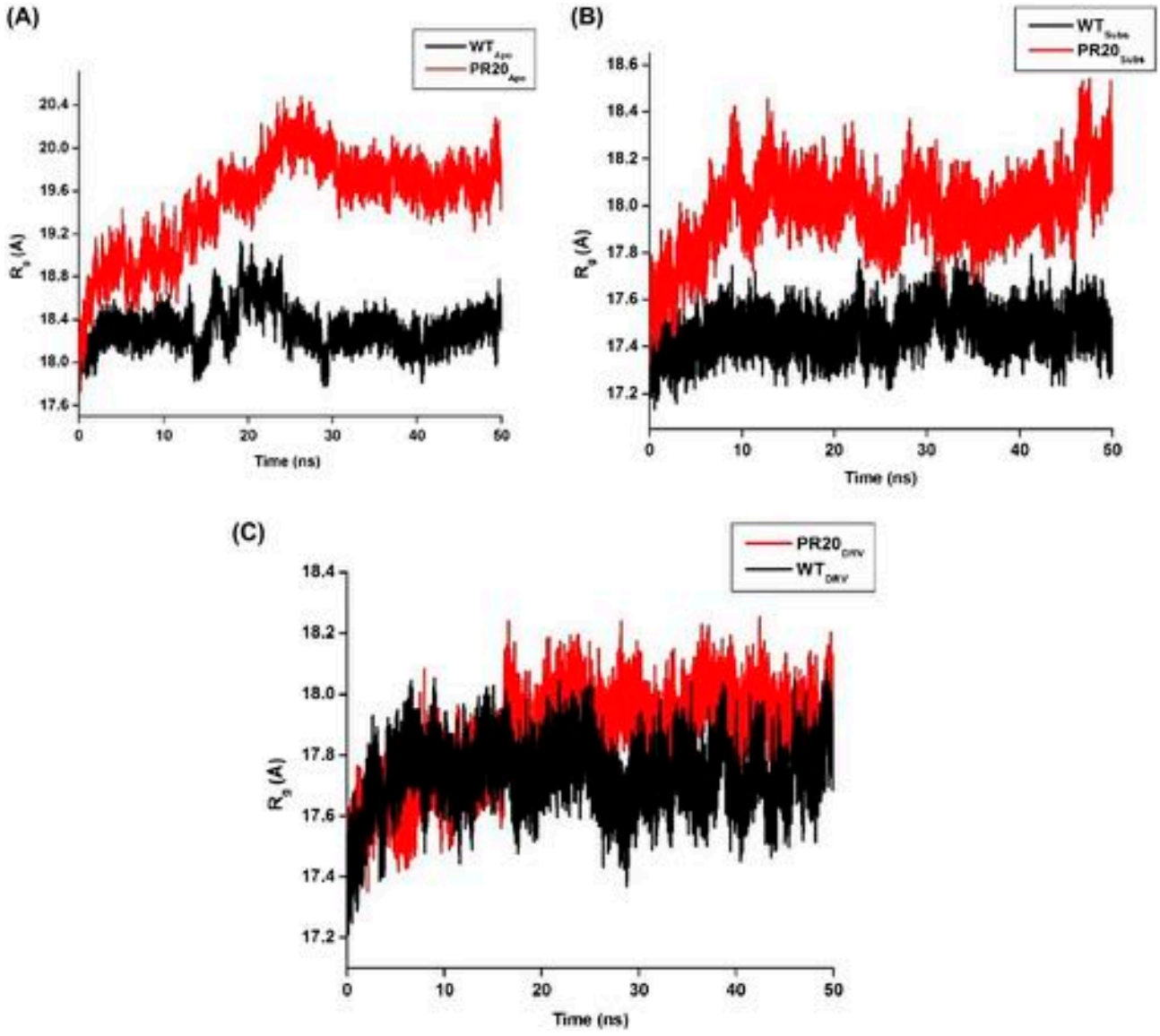

Figure 8. Deviations in the radius of gyration (R_g) during the simulation period. A, B and C highlight deviations in R_g in the case of WT_{apo}/$Pr20_{apo}$, WT_{Subs}/$PR20_{Subs}$ and WT_{DRV}/$PR20_{DRV}$, respectively.

covariance matrix of the Cα atomic fluctuations is .014 and –.21 Å for the WT and the mutant, respectively, indicating an overall change in amino acid residue motion in both systems. PCA showed that the occurrence of 20 mutations led to changes in the direction of motion across the first two normal modes (Figure S4 in Supplementary Materials). Normal mode analysis of WT_{DRV} and $PR20_{DRV}$ was also carried out and the results showed a slightly higher mobility of the $PR20_{DRV}$ (average mobility of NM1 2.11 Å and NM2 5.12 Å) across the first two normal modes (Figure 11(C) and (D)) as compared to WT_{DRV} (average mobility of NM1 2.10 Å and for NM2 4.46 Å). These findings further correlate with the outcomes from the RMSF and R_g parameters and highlight an overall conformational flexibility of DRV-bound HIV-PR as a result of 20 mutations which decreases the grip of protease on inhibitor and leads to a decrease in the binding free energy.

3.3. *Impact of mutations on drug binding landscape*

3.3.1. Binding free energy and energy decomposition analysis

To gain insight into the impact of mutation upon drug binding, post-dynamic binding free energy calculations using the MM/GBSA approach were performed (see Methods sections) for four systems (WT_{Sub}, WT_{DRV}, $PR20_{Sub}$ and $PR20_{DRV}$) – different ligands with determined experimental data (ΔG_{exp}) were used to ensure the validity of results.

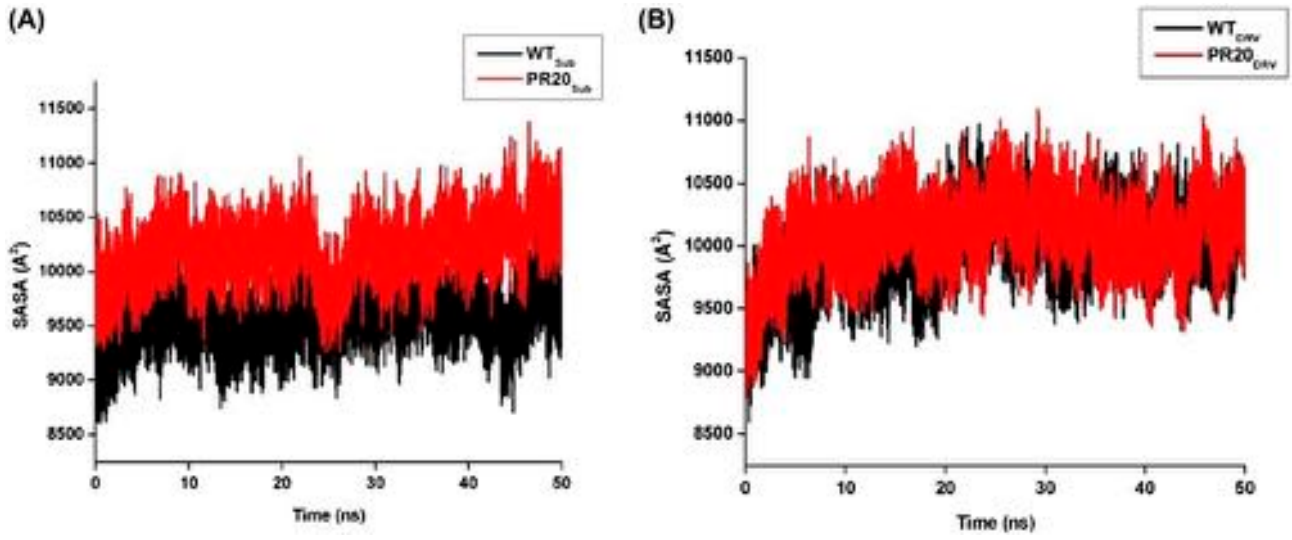

Figure 9. Fluctuation in the SASA for substrate-bound (A) and darunavir-bound (B) conformations during simulation time.

Table 2. MM/GBSA-based binding free energy profile of WT_{Sub}, $PR20_{Sub}$ (italics), WT_{DRV}, and $PR20_{DRV}$ (italics). The time-dependent fluctuation of ΔG_{bind} (kcal/mol)^{calc} is presented in Figure S6, Supplementary Materials.

HIV-PR complexes	E_{vdw}	E_{elec}	ΔG_{solv}	ΔG_{gas}	ΔG_{bind}(kcal/mol)$^{calc.}$	ΔG_{bind} (kcal/mol)$^{Exp.}$
WT_{sub}	−88.76 ± .29	−103.86 ± .47	107.29 ± .39	−192.63 ± .51	−85.34 ± .28	Not available
$PR20_{Sub}$	*−74.08 ± .19*	*−16.34 ± .23*	*30.22 ± .16*	*−90.43 ± .42*	*−60.17 ± .18*	Not available
WT_{DRV}	−56.65 ± .16	−9.26 ± .15	15.99 ± .12	−65.91 ± .23	−49.92 ± .16	−12.1 ± .8[a]
$PR20_{DRV}$	*−53.14 ± .19*	*−10.3 ± .16*	*18.79 ± .15*	*−63.4 ± .3*	*−44.65 ± .19*[c]	*−7.61 ± .11*[b]

Note: c and a (Mittal et al., 2013), b (Agniswamy et al., 2013) denotes calculated and experimental binding free energy, respectively.

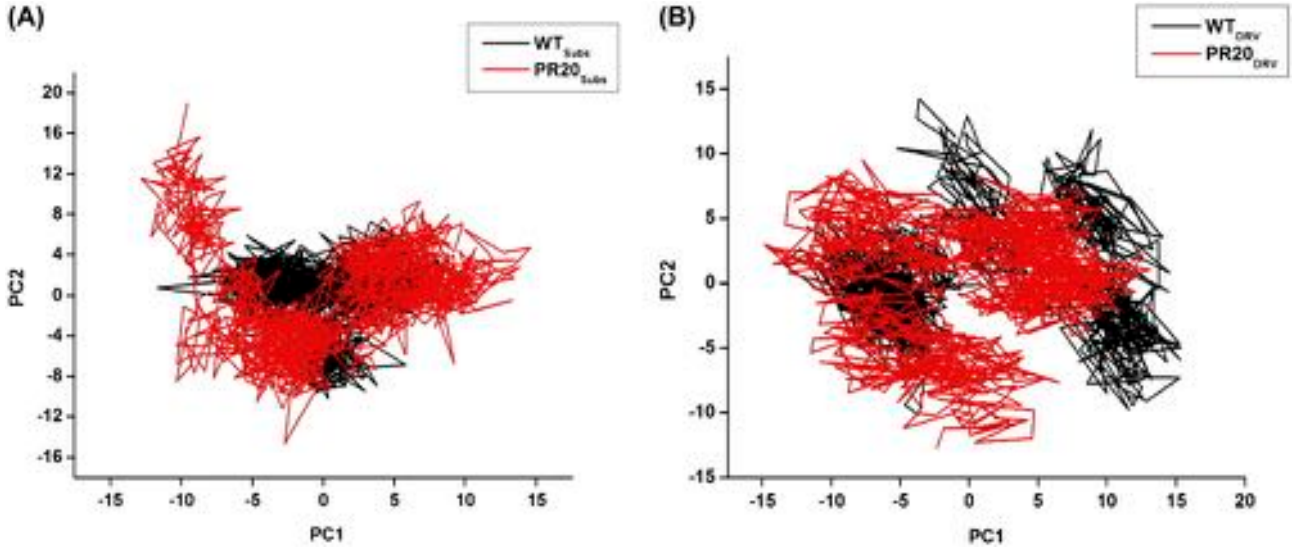

Figure 10. PCA showing difference in motion across the first two principal components (PC1 and PC2) for substrate- and darunavir-bound complexes of wild and PR20 variant of HIV-PR.

The binding free energy for $PR20_{Sub}$ and $PR20_{DRV}$ was higher in the case of the mutant (PR20) by ~25.17 kcal/mol and ~5.27 kcal/mol when compared to WT_{Sub} and WT_{DRV}, respectively.

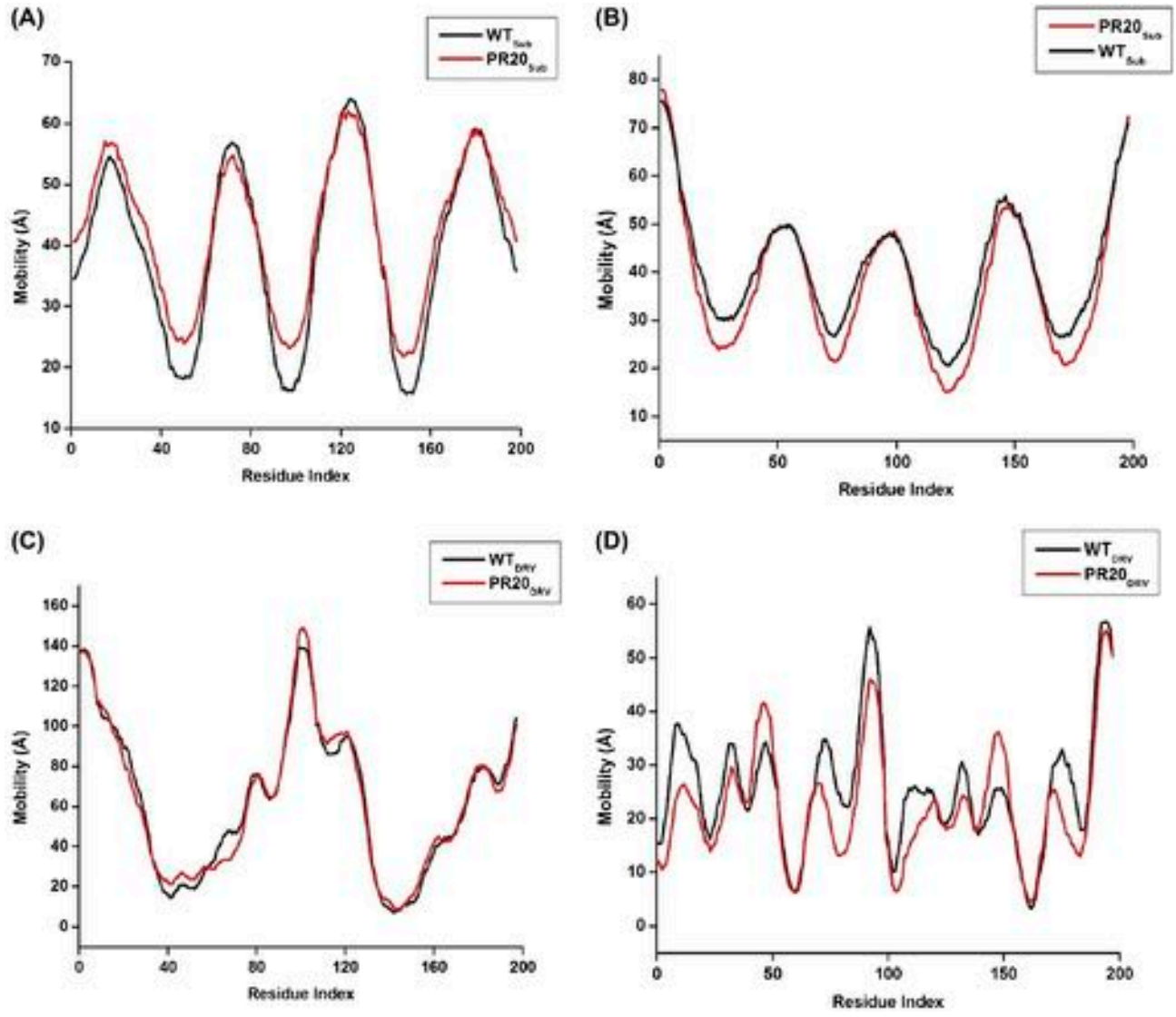

Figure 11. Per-residue fluctuations during the first two normal modes for $WT_{Sub/DRV}$ and $PR20_{Sub/DRV}$, respectively. A and B highlight differences in fluctuations across normal mode 1 and 2 for WT_{Sub} and $PR20_{Sub}$, respectively, whilst C and D highlight differences in fluctuations across normal mode I and II for WT_{DRV} and $PR20_{DRV}$.

Energy decomposition analysis (Table 2) showed that the van der Waals component was reduced by ~3.51 kcal/mol in the case of $PR20_{DRV}$ when compared to WT_{DRV}. The electrostatic and solvation contribution, however, increased by ~1.07 kcal/mol and ~2.8 kcal/mol, respectively. In both cases (wild and PR20 variant), it was observed that the greatest contribution to the total binding free energy came from the van der Waals components, thus it can be concluded that the van der Waals force is the major driving force behind binding and its reduction in the PR20 variant contributes the most to the overall decrease in binding free energy.

3.3.2. *Per-residue decomposition analysis*

Per-residue footprints were also computed to give a more detailed understanding of the mutational effect on the magnitude of the different binding forces. Per-residue footprints revealed a distinct difference in the interactions of the substrate with the active site residues of the wild-type and PR20 variant of HIV-PR (Figure 13). In the wild type, Asp25 and Asp 124 are catalytic residues, which form a key H-bond with the substrate, thereby holding it in place. This H-bond interaction, however, is lost in the mutant.

In the PR20 variant, we found that Asp 124 still plays a major role, but the contribution from Asp25 has

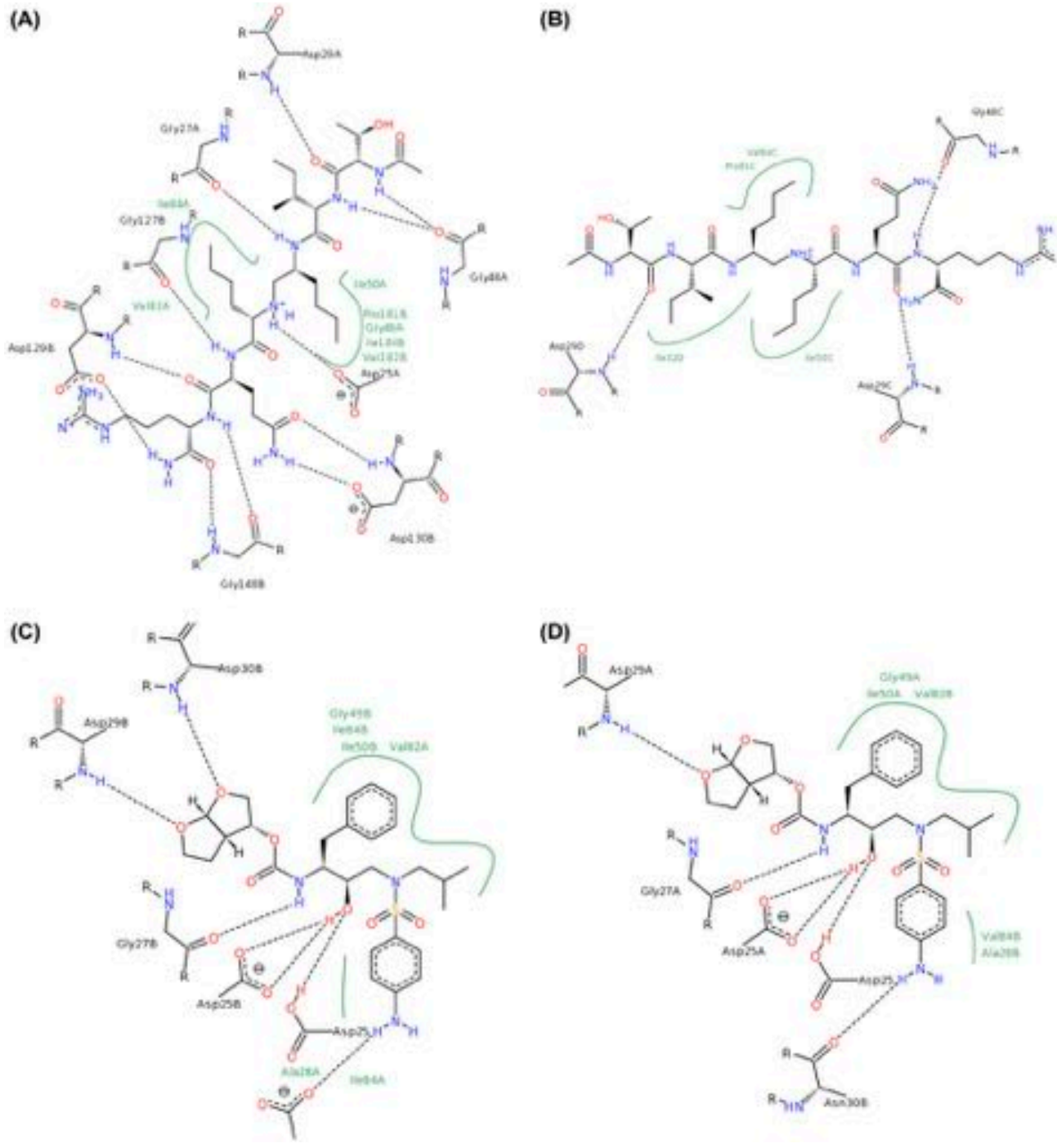

Figure 12. 2D ligand interaction plot highlighting interaction of active site residues with WT_{Subs} (A), $PR20_{Subs}$ (B), WT_{DRV} (C) and $PR20_{DRV}$ (D).

been substantially reduced. There is an almost symmetrical contribution from Asp25 and Asp124, Asp29 and Asp128, Asp30 and Asp129 in the wild type. This, however, changes in the PR20 variant, where the interactions were more asymmetrical resulting in greater interactions from Ala28, Asn30, Ile32, Lys45, Val47, Gly48, Gly49, Ile50, Leu70, Thr80, Pro81, Val82, Val84, Gly126, Ala127, Asn129, Ile131, Val146, Gly148, Pro180 and Val183. These residues contribute mainly to the overall van der Waals contribution. In the mutant, there is also a substantial drop in the electrostatic contribution from Asp25, Asp29, Asn30, Asp124, Asp128 and Asp129, where a difference of –56.31, –17.46, –14.77, –53.27, –15.22, –13.76 kcal/mol, for each of these respective

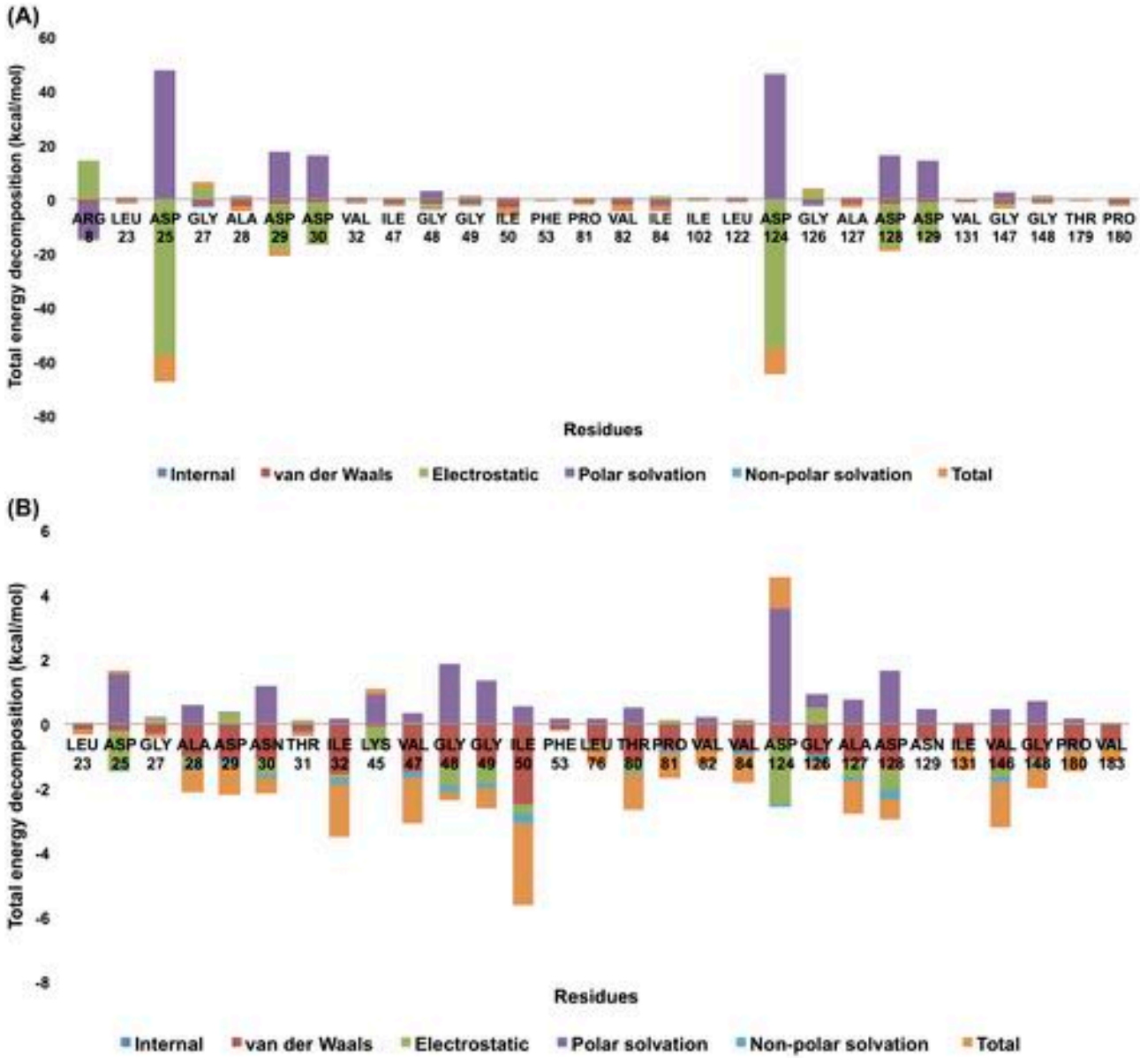

Figure 13. Per-residue decomposition profiles of the WT_{Sub} (A) and $PR20_{Sub}$ (B) using the MM/GBSA approach.

residues was observed. For residues, Asp25 and Asp124, a difference of –9.70 kcal/mol and –10.33 kcal/mol, respectively, towards the total energy contributions was detected. Mutated residues, D30N, V32I, I84V and I47V, which occur within the active site, cause a difference of –0.57, –1.16, –0.66 and –0.39 kcal/mol to their respective total energy contributions. The mutations, D30N, V32I and I47V, contributed to an increase in the total energy, whereas the I84V mutation led to a decrease in the total energy contribution.

In the case of the DRV-bound complex, a loss/change in H-bond interaction was observed as a result of mutations. In the wild type, Asp30 forms a direct H-bond interaction with the aniline group of DRV, whereas in the case of PR20 variant, the Asn side chain of the D30N forms a H-bond with DRV (Agniswamy et al., 2012) (Figure 12(C) and (D)). Furthermore, a loss of H-bond interaction was observed between the oxygen atom of oxathiolane ring with that of Asp130. The mutations were found to further affect the residues involved in the van der Waals interactions as highlighted in Figure 13(C) and (D).

For the DRV-bound conformation, a difference of 0.51 and –0.58 kcal/mol, respectively, for the total energy contribution was observed for residues Asp25 and Asp124 between the native wild type and the PR20 variant. Interestingly, an increased contribution from Asp25 was counteracted by a decreased contribution

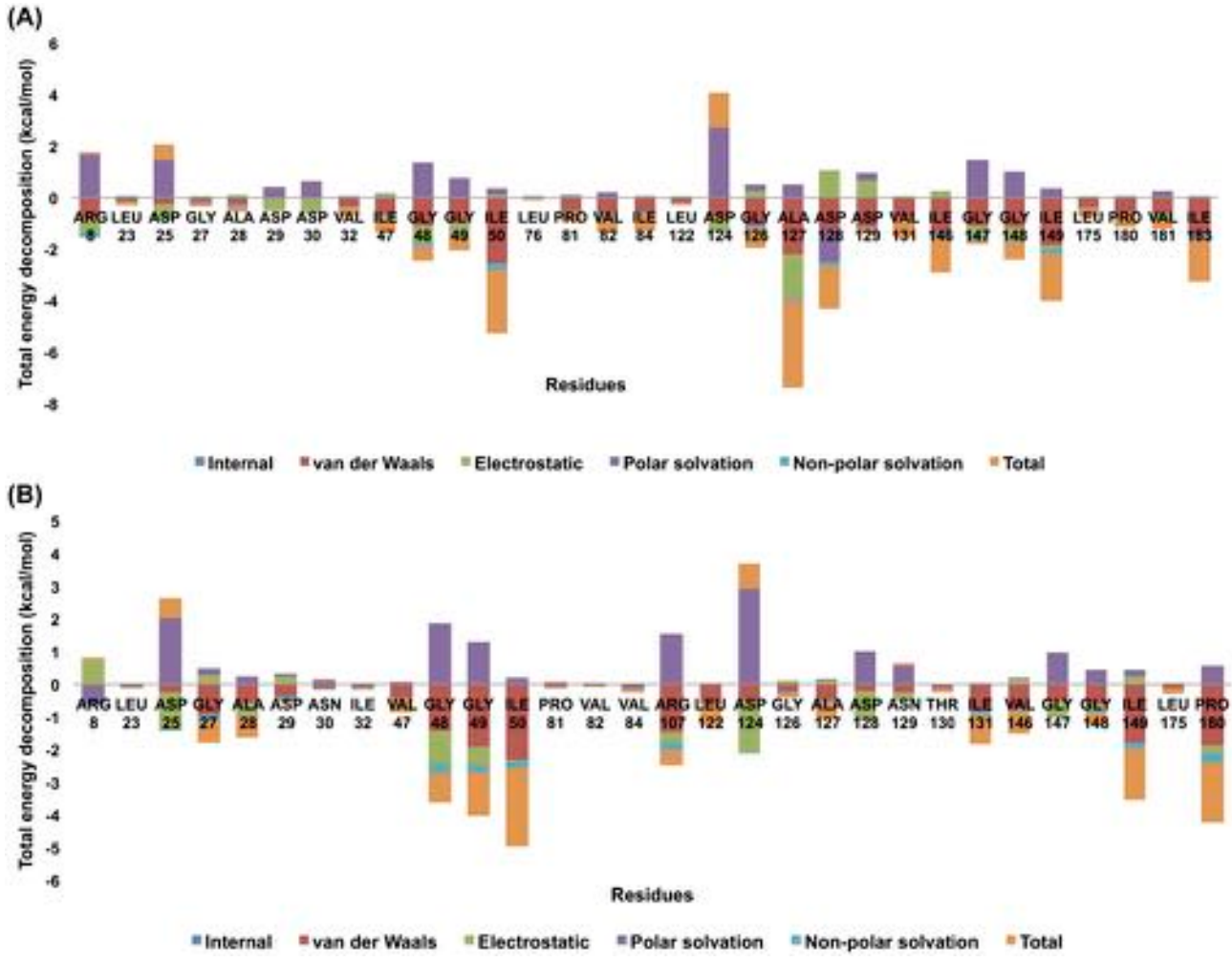

Figure 14. Per-residue decomposition profile of the WT_{DRV} (A) and $PR20_{DRV}$ (B) using the MM/GBSA approach.

Table 3. The effect of mutations in terms of lost and new residue–residue connections in the case of PR20 variant when compared with wild variant[a]. The graphical representations of RINs were presented as supplementary materials.

Lost connections	New connections
13:ILE (H-bond:mc-mc) 20:LYS	113:LYS (ionic:sc-sc) 164:GLU
14:ARG (ionic:sc-sc) 65:GLU	119:LYS (π-cation:sc-sc)132:PHE
57:ARG (ionic:sc-sc) 35:GLU	20:LYS (H-bond:mc-sc) 35:ASP
38:LEU (H-bond:mc-mc) 36:MET	83:ASN (H-bond:sc-sc) 35:ASP
57:ARG (H-bond:mc-sc) 36:MET	16:GLY (H-bond:mc-mc) 63:PRO
88:ASN (H-bond:mc-mc) 29:ASP	92:GLN (H-bond:mc-sc) 88:ASP
88:ASN (H-bond:mc-sc) 74:THR	130:THR (H-bond:mc-sc) 187:ASP
187:ASN (H-bond:mc-sc) 173:THR	31:THR (H-bond:sc-sc) 89:THR
93:ILE (H-bond:mc-mc) 89:LEU	130:THR (H-bond:sc-sc) 188:THR
192:ILE (H-bond:mc-mc) 188:LEU	43:LYS (ionic:sc-sc) 58:GLU
194:ALA (hbond:mc-mc) 189:LEU	
69:HIS (π-π stack:sc-sc) 198:PHE	
8:ARG (ionic:sc-sc) 128:ASP	
107:ARG (ionic:sc-sc) 29:ASP	
119:LYS (ionic:sc-sc) 133:GLU	
99:PHE (π-π stack:sc-sc) 168:HIS	

[a]sc – side chain, mc – main chain.

from Asp124. It was also observed that the active site mutations, D30N, V32I, I84V and I47V, led to a decrease in 0.05, –0.26, –0.53 and –0.55 kcal/mol to their respective total energy contributions (Figure 13).

The reduction in the number of hydrogen bonds, changes in van der Waals connections as well as a decreased magnitude in the per-residue energy decomposition as a result of mutation, combines to influence the drug binding landscape which ultimate affects the overall conformational dynamics of the wild and PR20 variant of HIV-PR.

3.4. RIN profile

The occurrence of mutations in the protein backbone leads to changes in residue–residue connections, which is presumed to be one of the main reasons for changes in the conformational landscape (Bhakat et al., 2014; Karubiu et al., 2014). The presence of 20 mutations leads to significant changes in residue–residue connections, which is highlighted in Table 3 (Figure S7–S11 in Supplementary Materials). It is quite clear from the RIN network that there are slightly fewer hydrogen bond networks in the case of PR20 as compared to the wild-type variant. Most of the losses are compensated for with the exception of a few. These changes in inter-residue connections resulted in an increased flexibility of PR20 variant which contributes towards a distorted ligand binding landscape, loss in binding free energy as well as an alteration in the conformational behaviour of HIV-PR.

4. Conclusion

The detailed analyses provided in this report show that the presence of 20 mutations significantly impacts on the change in the conformational and drug binding landscape of the HIV protease. Molecular dynamic simulations on the apo conformation of the wild and the PR20 variants revealed that these 20 mutations had a profound effect on flap opening and closing, altering it from a "symmetrical" motion to an "asymmetrical" one, leading us to speculate that this difference in motion contributes to an overall decrease in dimer association, possibly contributing to a drop in drug/substrate binding potential. This finding was validated by the fact that the dimer dissociation constant (K_d) for $PR20_{Sub}$ exhibited a 30-fold decrease when compared to WT_{Sub} (Agniswamy et al., 2012). The higher fluctuation in both the per-residue analyses, as well as distance between flap tips of the apo structure of the PR20 in comparison to the wild type, confirms a gain in conformational flexibility as a result of mutation. The mutations led to a loss of several residue–residue interactions which led to an increased flexibility in the case of PR20 variant. The increase in RMSF led to a loss of enzyme grip on inhibitor which affects the binding landscape of inhibitors which is evident from a decreased binding free energy in the case of the PR20 variant. Interpretation of the radius of gyration, PCA and SASA data provided useful insight into the effect of the mutations on the overall dynamics and changes to the hydrophobic core. It is worth mentioning that the RMSF, R_g and NMR mobility plot in the case of $PR20_{DRV}$ are very similar to that of WT_{DRV} with just a slightly increased mobility in the regions where PR20 mutations occurred. This can be further validated by the fact that the difference in calculated/experimental binding free energy in the case of $PR20_{DRV}$ is slightly less than WT_{DRV} and better than $PR20_{Subs}$. This fact further proves the effectiveness of DRV in inhibiting the PR20 variant. Thus, discovering the development of new analogues of DRV might lead to a potent inhibitor which can inhibit MDR strains to a greater extent. Drug discovery targeting the HIV protease still remains a key interest in modern drug discovery. The findings reported in this study will significantly help in the rational design of post-darunavir novel HIV-PR inhibitors with an improved potency, targeted towards various MDR strains.

Supplementary material

The RMSDs, potential energies and graphical representation of RIN profiles as well as Cytoscape sessions of RINs were presented as Supplementary Materials. The supplementary material for this paper is available online at http://dx.doi.10.1080/07391102.2015.1018326.

Acknowledgement

SC, SB and MES acknowledge Centre of High Performance Computing (CHPC), Cape Town and School of Health Sciences, University of KwaZulu-Natal for technical and financial supports. AJMM acknowledges his funding agencies Proyecto Anillo ACT-1107 and Proyecto Basal FCV PFB16.

Conflicts of interest

Authors declare no potential conflicts of interest.

References

Agniswamy, J., Shen, C. H., Aniana, A., Sayer, J. M., Louis, J. M., & Weber, I. T. (2012). HIV-1 protease with 20 mutations exhibits extreme resistance to clinical inhibitors through coordinated structural rearrangements. *Biochemistry, 51*, 2819–2828.

Agniswamy, J., Shen, C. H., Wang, Y. F., Ghosh, A. K., Rao, K. V., Xu, C. X., … Weber, I. T. (2013). Extreme multi-drug resistant HIV-1 protease with 20 mutations is resistant to novel protease inhibitors with P1′-pyrrolidinone or P2-tris-tetrahydrofuran. *Journal of Medicinal Chemistry, 56*, 4017–4027.

Ahmed, S. M., Kruger, H. G., Govender, T., Maguire, G. E. M., Sayed, Y., Ibrahim, M. A. A., … Soliman, M. E. S. (2013). Comparison of the molecular dynamics and calculated binding free energies for nine FDA-approved HIV-1 PR drugs against subtype B and C-SA HIV PR. *Chemical Biology & Drug Design, 81*, 208–218.

Ahmed, S. M., Maguire, G. E. M., Kruger, H. G., & Govender, T. (2014). The impact of active site mutations of South African HIV PR on drug resistance: Insight from molecular dynamics simulations, binding free energy and per-residue footprints. *Chemical Biology & Drug Design, 83*, 472–481.

Bauer-Mehren, A. (2013) Integration of genomic information with biological networks using Cytoscape. *Methods in Molecular Biology (Clifton, N.J.), 1021*, 37–61.

Bennett, D. E., Camacho, R. J., Otelea, D., Kuritzkes, D. R., Fleury, H., Kiuchi, M., … Shafer, R. W. (2009). Drug resistance mutations for surveillance of transmitted HIV-1 drug-resistance: 2009 update. *PloS One, 4*, e4724.

Bhakat, S., Martin, A. J. M., & Soliman, M. E. S. (2014). An integrated molecular dynamics, principal component analysis and residue interaction network approach reveals the impact of M184V mutation on HIV reverse transcriptase resistance to lamivudine. *Molecular Biosystems, 10*, 2215–2228.

Brik, A. & Wong, C. H. (2003). HIV-1 protease: Mechanism and drug discovery. *Organic & Biomolecular Chemistry, 1*, 5–14.

Case, D. A., Cheatham, T. E., Darden, T., Gohlke, H., Luo, R., Merz, K. M., … Woods, R. J. (2005). The Amber biomolecular simulation programs. *Journal of Computational Chemistry, 26*, 1668–1688.

Doncheva, N. T., Klein, K., Domingues, F. S., & Albrecht, M. (2011). Analyzing and visualizing residue networks of protein structures. *Trends in Biochemical Sciences, 36*, 179–182.

Doss, C. G. P., Rajith, B., Chakraboty, C., Balaji, V., Magesh, R., Gowthami, B., … Das, M. (2014). In silico profiling and structural insights of missense mutations in RET protein kinase domain by molecular dynamics and docking approach. *Molecular Biosystems, 10*, 421–436.

Flexner, C. (2007). HIV drug development: The next 25 years. *Nature Reviews Drug Discovery, 6*, 959–966.

Foulkes-Murzycki, J. E., Rosi, C., Yilmaz, N. K., Shafer, R. W., & Schiffer, C. A. (2013). Cooperative effects of drug-resistance mutations in the flap region of HIV-1 protease. *ACS Chemical Biology, 8*, 513–518.

Freedberg, D. I., Ishima, R., Jacob, J., Wang, Y.-X., Kustanovich, I., Louis, J. M., & Torchia, D. A. (2002). Rapid structural fluctuations of the free HIV protease flaps in solution: Relationship to crystal structures and comparison with predictions of dynamics calculations. *Protein Science, 11*, 221–232.

Heal, J. W., Jimenez-Roldan, J. E., Wells, S. A., Freedman, R. B., & Romer, R. A. (2012). Inhibition of HIV-1 protease: The rigidity perspective. *Bioinformatics, 28*, 350–357.

Heaslet, H., Rosenfeld, R., Giffin, M., Lin, Y.-C., Tam, K., Torbett, B. E., … Stout, C. D. (2007). Conformational flexibility in the flap domains of ligand-free HIV protease. *Acta Crystallographica Section D-Biological Crystallography, 63*, 866–875.

Hornak, V., Okur, A., Rizzo, R. C., & Simmerling, C. (2006a). HIV-1 protease flaps spontaneously open and reclose in molecular dynamics simulations. *Proceedings of the National Academy of Sciences United States of America, 103*, 915–920.

Hornak, V., Okur, A., Rizzo, R. C., & Simmerling, C. L. (2006b) Flap structure and dynamics in HIV-1 protease simulations. *Abstracts of Papers of the American Chemical Society, 231*, 915–920.

Hornak, V., Okur, A., Rizzo, R. C., & Simmerling, C. (2006c). HIV-1 protease flaps spontaneously close to the correct structure in simulations following manual placement of an inhibitor into the open state. *Journal of the American Chemical Society, 128*, 2812–2813.

Hornak, V., & Simmerling, C. (2007). Targeting structural flexibility in HIV-1 protease inhibitor binding. *Drug Discovery Today, 12*, 132–138.

Kamaraj, B., & Purohit, R. (2013). In silico screening and molecular dynamics simulation of disease-associated nsSNP in TYRP1 gene and its structural consequences in OCA3. *Biomed Research International, 2012*, 1–13.

Karthik, S., & Senapati, S. (2011). Dynamic flaps in HIV-1 protease adopt unique ordering at different stages in the catalytic cycle. *Proteins-Structure Function and Bioinformatics, 79*, 1830–1840.

Karubiu, W., Bhakat, S., & Soliman, M. S. (2014). Compensatory role of double mutation N348I/M184V on nevirapine binding landscape: Insight from molecular dynamics simulation. *Protein Journal, 5*, 1–15.

Leonis, G., Steinbrecher, T., & Papadopoulos, M. G. (2013). A contribution to the drug resistance mechanism of darunavir, amprenavir, indinavir, and saquinavir complexes with HIV-1 protease due to flap mutation 150V: A systematic MM-PBSA and thermodynamic integration study. *Journal of Chemical Information and Modeling, 53*, 2141–2153.

Liu, F. L., Kovalevsky, A. Y., Tie, Y. F., Ghosh, A. K., Harrison, R. W., & Weber, I. T. (2008). Effect of flap mutations on structure of HIV-1 protease and inhibition by saquinavir and darunavir. *Journal of Molecular Biology, 381*, 102–115.

Makatini, M., Petzold, K., Alves, C., Arvidsson, P., Honarparvar, B., Govender, P., … Soliman, M. (2013). Synthesis, 2D-NMR and molecular modelling studies of pentacycloundecane. *Journal of Enzyme Inhibition and Medicinal Chemistry, 28*, 78–88.

Mehellou, Y. & De Clercq, E. (2010). Twenty-six years of anti-HIV drug discovery: Where do we stand and where do we go? *Journal of Medicinal Chemistry, 53*, 521–538.

Mittal, S., Bandaranayake, R. M., King, N. M., Prabu-Jeyabalan, M., Nalam, M. N. L., Nalivaika, E. A., … Schiffer, C. A. (2013). Structural and thermodynamic basis of amprenavir/darunavir and atazanavir resistance in HIV-1 protease with mutations at residue 50. *Journal of Virology, 87*, 4176–4184.

Mittal, S., Cai, Y., Nalam, M. N. L., Bolon, D. N. A., & Schiffer, C. A. (2012). Hydrophobic core flexibility modulates enzyme activity in HIV-1 Protease. *Journal of the American Chemical Society, 134*, 4163–4168.

Molla, A., Korneyeva, M., Gao, Q., Vasavanonda, S., Schipper, P. J., Mo, H. M., … Kempf, D. J. (1996). Ordered accumulation of mutations in HIV protease confers resistance to ritonavir. *Nature Medicine, 2*, 760–766.

Muzammil, S., Ross, P., & Freire, E. (2003). A major role for a set of non-active site mutations in the development of HIV-1 protease drug resistance. *Biochemistry, 42*, 631–638.

Naicker, P., Achilonu, I., Fanucchi, S., Fernandes, M., Ibrahim, M. A. A., Dirr, H. W., … Sayed, Y. (2013). Structural insights into the South African HIV-1 subtype C protease: Impact of hinge region dynamics and flap flexibility in drug resistance. *Journal of Biomolecular Structure and Dynamics, 31*, 1370–1380.

Perryman, A. L., Lin, J. H., & McCammon, J. A. (2004). HIV-1 protease molecular dynamics of a wild-type and of the V82F/I84V mutant: Possible contributions to drug resistance and a potential new target site for drugs (vol 13, pg 1108, 2004). *Protein Science, 13*, 1434–1434.

Pettersen, E. F., Goddard, T. D., Huang, C. C., Couch, G. S., Greenblatt, D. M., Meng, E. C., & Ferrin, T. E. (2004). UCSF chimera – A visualization system for exploratory research and analysis. *Journal of Computational Chemistry, 25*, 1605–1612.

Piana, S., Carloni, P., & Rothlisberger, U. (2002). Drug resistance in HIV-1 protease: Flexibility-assisted mechanism of compensatory mutations. *Protein Science, 11*, 2393–2402.

Rhee, S. Y., Taylor, J., Fessel, W. J., Kaufman, D., Towner, W., Troia, P., … Shafer, R. W. (2010). HIV-1 protease mutations and protease inhibitor cross-resistance. *Antimicrobial Agents and Chemotherapy, 54*, 4253–4261.

Roe, D. R., & Cheatham III, T. E. (2013). PTRAJ and CPPTRAJ: Software for processing and analysis of molecular dynamics trajectory data. *Journal of Chemical Theory and Computation, 9*, 3084–3095.

Scott, W. R. P. & Schiffer, C. A. (2000). Curling of flap tips in HIV-1 protease as a mechanism for substrate entry and tolerance of drug resistance. *Structure, 8*, 1259–1265.

Shenai, P. M. X. & Zhao, Z. (2012). Applications of Principal Component Analysis (PCA) in Materials Science. In P. Sanguansat (Ed.), *Principal component analysis-engineering applications* (pp. 1–40). InTech. ISBN: 978-953-51-0182-6. Retrieved from http://www.intechopen.com/books/principal component-analysis-engineering-applications/applications-of-principal-component-analysis-pca-in-materialsscience

Spinelli, S., Liu, Q. Z., Alzari, P. M., Hirel, P. H., & Poljak, R. J. (1991). The 3-dimensional structure of the aspartyl protease from the HIV-1 isolate bru. *Biochimie, 73*, 1391–1396.

Tie, Y. F., Boross, P. I., Wang, Y. F., Gaddis, L., Liu, F. L., Chen, X. F., … Weber, I. T. (2005). Molecular basis for substrate recognition and drug resistance from 1.1 to 1.6 angstrom resolution crystal structures of HIV-1 protease mutants with substrate analogs. *FEBS Journal, 272*, 5265–5277.

von der Helm, K. (1996). Retroviral proteases: Structure, function and inhibition from a non-anticipated viral enzyme to the target of a most promising HIV therapy. *Biological Chemistry, 377*, 765–774.

Walsh, I., Martin, A. J. M., Di Domenico, T., & Tosatto, S. C. E. (2012). ESpritz: Accurate and fast prediction of protein disorder. *Bioinformatics, 28*, 503–509.

Wlodawer, A. & Vondrasek, J. (1998). Inhibitors of HIV-1 protease: A major success of structure-assisted drug design. *Annual Review of Biophysics and Biomolecular Structure, 27*, 249–284.

Zhang, Y., Chang, Y.-C. E., Louis, J. M., Wang, Y.-F., Harrison, R. W., & Weber, I. T. (2014). Structures of darunavir-resistant HIV-1 protease mutant reveal atypical binding of darunavir to wide open flaps. *ACS Chemical Biology, 9*, 1351–1358.

Zhang, Y. M., Imamichi, H., Imamichi, T., Lane, H. C., Falloon, J., Vasudevachari, M. B., & Salzman, N. P. (1997). Drug resistance during Indinavir therapy is caused by mutations in the protease gene and in its Gag substrate cleavage sites. *Journal of Virology, 71*, 6662–6670.

Zhu, Z. W., Schuster, D. I., & Tuckerman, M. E. (2003). Molecular dynamics study of the connection between flap closing and binding of fullerene-based inhibitors of the HIV-1 protease. *Biochemistry, 42*, 1326–1333.